
Article:
Chen, L., Wang, Z. orcid.org/0000-0002-4054-0533, Li, B. orcid.org/0000-0002-1100-2058 et al. (1 more author) (2023) Computation of the crack opening displacement in the phase-field model. International Journal of Solids and Structures, 283. 112496. ISSN 0020-7683

https://doi.org/10.1016/j.ijsolstr.2023.112496

International Journal of Solids and Structures 283 (2023) 112496

Contents lists available at ScienceDirect

International Journal of Solids and Structures

journal homepage: www.elsevier.com/locate/ijsolstr

Computation of the crack opening displacement in the phase-field model

Lin Chen [a], Zhao Wang [c], Bin Li [b], René de Borst [c,*]

[a] Northeastern University, Key Laboratory of Ministry of Education on Safe Mining of Deep Metal Mines, Shenyang 110819, China
[b] Guangdong Technion-Israel Institute of Technology, Department of Mechanical Engineering, Shantou 515063, China
[c] University of Sheffield, Department of Civil and Structural Engineering, Sir Frederick Mappin Building, Mappin Street, Sheffield S1 3JD, UK

ARTICLE INFO

Keywords:
Crack opening
Phase field model
Brittle fracture
Cohesive fracture
Smeared crack

ABSTRACT

The phase-field model treats discrete cracks in a smeared sense by a regularisation technique. It holds attractive properties: there is no need to consider cracks as geometric discontinuities, and it avoids remeshing around crack tips. The method has been employed in the analysis of brittle and cohesive fracture problems. In the brittle fracture model, a Griffith-like energy functional is used in the simulation, while in the cohesive fracture model, the fracturing problem exploits a displacement jump governed energy functional. Obviously, the displacement jump is crucial in the cohesive fracture model and in certain other applications, e.g. for hydraulic fracturing. In the current study, the approximated form of the crack opening displacement is derived for the brittle and cohesive fracture models. In both models, the crack opening displacement is associated with a line integral normal to the crack, but different factors in front of the integral apply. The derived integrals are verified analytically in a one-dimensional setting and numerically in multi-dimensional set-ups, featuring straight and curved cracks.

1. Introduction

Phase field models have become popular for fracturing analysis since its initial work by Francfort and Marigo (1998) and Bourdin et al. (2000). It describes the crack by a scalar phase field variable. Different from discrete crack models, e.g., Chen et al. (2017), cracks are descried in a smeared sense in phase-field models, so that there is no need to treat cracks as geometric discontinuities and remeshing around crack tips is avoided. In the phase-field approach to brittle fracture, crack initiation and quasi-static propagation are considered as an energy functional minimisation problem. To be suitable for large-scale computations, a regularisation strategy was developed by Bourdin et al. (2008), which transforms the sharp discontinuity into a smeared crack, governed by a phase-field variable d. The width of the smeared crack is set by an internal length scale ℓ (Bourdin et al., 2000).

The vast majority of phase-field models have been applied in the analysis of brittle fracture, e.g. Heider (2021). Its application spans from ductile fractures (Miehe et al., 2015) to fatigue analysis (Alessi et al., 2018), hydraulic fracturing (Chukwudozie et al., 2019), and dynamic fracture (Li et al., 2016). Different from the external load induced fracture, hydraulic fracturing is a physical process caused by the fluid pressure in the crack (Yoshioka et al., 2020). To consider the effect of the fluid flow in the crack, the Reynolds flow model is typically employed in the analysis (Miehe and Mauthe, 2016). Generally, the Reynolds flow model strongly depends on the crack opening displacement, e.g., the cubic law for the fluid velocity. The extension of the phase-field approach to cohesive fracture has been addressed by Verhoosel and de Borst (2013) and by Nguyen et al. (2016), employing a displacement jump dependent energy functional in the analysis, see also Vignollet et al. (2014), May et al. (2015), Ghaffari Motlagh and de Borst (2020) and Chen and de Borst (2022). Obviously, the displacement jump, including the crack opening displacement in the crack normal direction and the displacement jump in the crack shear direction, is a crucial variable in the cohesive fracture model and also in certain other applications such as hydraulic fracturing.

So far, the computation of the displacement jump in the shear direction is underdeveloped, while for the computation of the crack opening several approaches are available (Heider, 2021). In the early work on the analysis of hydraulic fracturing by brittle phase-field models, a line integral was used to compute the crack opening in the direction normal to the crack (Bourdin et al., 2012). Later, Chukwudozie et al. (2019) and Yoshioka et al. (2020) have theoretically proven the integral formula in the framework of the brittle fracture model, and have detailed the implementation of the integral form.

Verhoosel and de Borst (2013) proposed a cohesive phase field model which exploits an auxiliary field to model the displacement jump which is required as an input in a cohesive-zone model. More recently, Chen and de Borst (2022) have systematically studied the

* Corresponding author.
E-mail address: r.deborst@sheffield.ac.uk (R. de Borst).

https://doi.org/10.1016/j.ijsolstr.2023.112496
Received 16 March 2023; Received in revised form 7 September 2023; Accepted 26 September 2023
Available online 28 September 2023

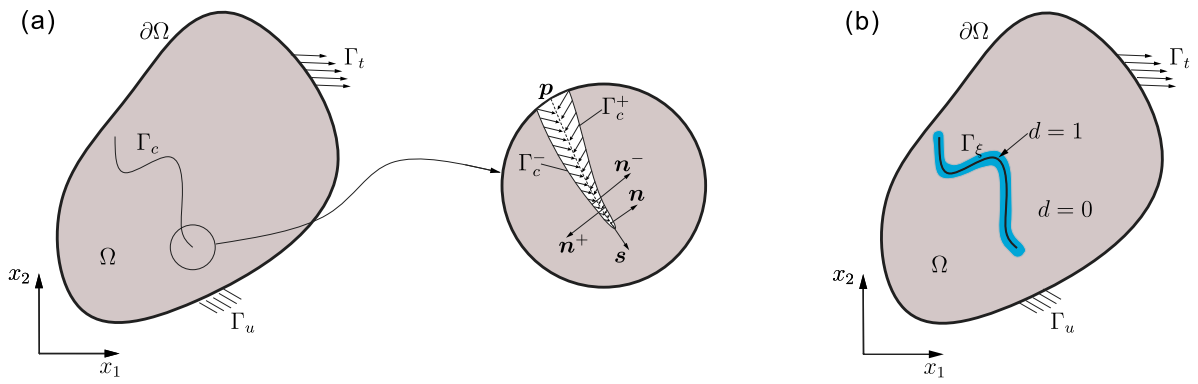

Fig. 1. (a) a solid body Ω with an internal crack Γ_c. Γ_c is an interface boundary with positive and negative sides, Γ_c^+ and Γ_c^-, respectively. Tractions $\boldsymbol{p}$ are prescribed along Γ_c. Boundary Γ_u is prescribed with a displacement $\bar{\mathbf{u}}$; Γ_t with a prescribed traction $\hat{\mathbf{t}}$; (b) a solid body Ω with a smeared crack Γ_ξ (blue area).

cohesive phase field model and proposed different forms of phase-field models. From their analysis, it appears that the auxiliary field should be prescribed in the whole domain, reducing the computational efficiency. Nguyen et al. (2016) avoided an auxiliary field by computing the displacement jump at two points near the interface. However, the choice of the location of these points seems arbitrary and problem-dependent. Lee et al. (2017) and Yoshioka et al. (2020) employed a level-set approach to compute the normal vector of the crack, which is used in the computation of the displacement jump at each quadrature point. Obviously, the accuracy of this approach relies on the choices of the level set function.

This study will address the general case of the computation of the crack opening displacement in the framework of phase-field modelling. The line integral form of crack opening displacement will be derived separately for the brittle and the cohesive fracture models. We will validate the proposed formula theoretically in a one-dimensional setting and numerically in multi-dimensional set-ups. We will start this contribution with a concise description of phase field modelling of fractures. Subsequently, the crack opening displacement is derived for the brittle and cohesive fracture model, respectively. The theoretical validation of the proposed formula is given in Section 4. Finally, two numerical examples are presented to numerically validate the approach and conclusions are drawn.

2. Phase field model for fracture

In this section, we will briefly elaborate on the phase-field modelling of brittle and cohesive fracture, see Fig. 1. The internal discontinuity Γ_c can either refer to a brittle or to a cohesive fracture. Tractions $\boldsymbol{p}$ on Γ_c can either by a fluid pressure applied on the brittle fracture surface, or cohesive tractions. In this contribution, infinitesimal strains, linear elastic material behaviour and the absence of body force have been assumed.

2.1. Phase field regularised brittle fracture model

The variational approach to brittle fracture was proposed by Francfort and Marigo (1998). The crack initiation and quasi-static evolution are governed by a minimisation of a Griffith-like energy functional. Here, we consider a cracked body $\Omega \subseteq \mathcal{R}^n$ with a prescribed tractions $\boldsymbol{p}$ on Γ_c, prescribed displacements $\bar{\mathbf{u}}$ on $\partial\Omega_u$, and a prescribed traction $\hat{\mathbf{t}}$ on $\partial\Omega_t$. Then, the total energy functional for the cracked body read (Yoshioka et al., 2020)

$$\mathcal{E}(\mathbf{u}, \Gamma; \boldsymbol{p}) = \mathcal{P}(\mathbf{u}, \Gamma; \boldsymbol{p}) + \mathcal{E}_s(\Gamma) = \mathcal{P}(\mathbf{u}, \Gamma; \boldsymbol{p}) + \mathcal{G}_c \int_\Gamma \mathrm{d}\mathcal{H}^{n-1}, \tag{1}$$

where $\mathcal{P}(\mathbf{u}, \Gamma; \boldsymbol{p})$ is the potential for the cracked body, including the strain energy, the work done by the externally applied loads and the work from the tractions $\boldsymbol{p}$. $\mathcal{E}_s(\Gamma)$ represents the fracture surface energy in the sense of Griffith's theory of brittle fracture, $\mathcal{H}^{n-1}$ denotes the $(n-1)$-dimensional Hausdorff surface measure and Γ is the set of cracks where the displacement fields $\mathbf{u} \in H^1(\Omega \setminus \Gamma)$ can jump, $H^1(\Omega \setminus \Gamma)$ being the Sobolev space of functions with square integrable first derivative. $\mathcal{G}_c$ denotes a scaling factor, with the dimension of energy per unit surface.

In brittle fracture models tractions $\boldsymbol{p}$ can be considered as the pressure p_f exerted on the crack Γ_c, such as in the hydraulic fracturing (Chukwudozie et al., 2019; Yoshioka et al., 2020). The pressure p_f will induce work in the crack opening direction (Chen et al., 2022b). To elaborate the approach on how to compute the crack opening we will assume the traction $\boldsymbol{p}$ to be a pressure p_f exerted on the crack Γ_c. Correspondingly, the potential $\mathcal{P}(\mathbf{u}, \Gamma; \boldsymbol{p})$ for the cracked body is given as (Yoshioka et al., 2020)

$$\mathcal{P}(\mathbf{u}, \Gamma; \boldsymbol{p}) = \mathcal{P}(\mathbf{u}, \Gamma; p_f) = \int_{\Omega\setminus\Gamma} \mathcal{W}(\mathbf{u})\,\mathrm{d}\Omega - \int_{\Gamma_t} \mathbf{u}\cdot\hat{\mathbf{t}}\,\mathrm{d}\Gamma - \int_{\Gamma_c} p_f\,[\![\mathbf{u}\cdot\boldsymbol{n}]\!]\,\mathrm{d}\Gamma, \tag{2}$$

in which $\mathcal{W}(\mathbf{u})$ is the energy density function and $\hat{\mathbf{t}}$ is the prescribed traction on the boundary Γ_t. In this contribution, we consider isotropic linear elasticity, such that $\mathcal{W}(\mathbf{u}) = \mu\boldsymbol{\varepsilon}(\mathbf{u})\cdot\boldsymbol{\varepsilon}(\mathbf{u}) + \lambda/2\mathrm{tr}(\boldsymbol{\varepsilon}(\mathbf{u}))^2$ with $\boldsymbol{\varepsilon}(\mathbf{u}) = 1/2\left(\nabla\mathbf{u} + \nabla\mathbf{u}^{\mathrm{T}}\right)$, λ and μ being Lamé constants, and $\cdot$ denotes the inner product. $[\![\mathbf{u}\cdot\boldsymbol{n}]\!]$ denotes the crack opening displacement, $[\![v_n]\!] = [\![\mathbf{u}\cdot\boldsymbol{n}]\!]$.

The direct numerical implementation of Griffith's energy functional (1) is challenging because of the unknown displacement jump location. We therefore resort to the regularisation strategy proposed by Bourdin et al. (2000), originally developed for image segmentation problems. In a regularised framework, cracks are represented by a scalar phase field variable d, ranging from 0 (away from the crack) to 1 (completely broken state). d varies smoothly in a band of finite width, resulting in a smeared vision of crack model. Then, the energy functional Eq. (1) is substituted by the functional:

$$\mathcal{E}(\mathbf{u}, \Gamma; \boldsymbol{p}) = \int_\Omega a(d)\,\mathcal{W}(\mathbf{u})\,\mathrm{d}\Omega - \int_{\Gamma_t} \mathbf{u}\cdot\hat{\mathbf{t}}\,\mathrm{d}\Gamma - \int_{\Gamma_c} p_f\,[\![\mathbf{u}\cdot\boldsymbol{n}]\!]\,\mathrm{d}\Gamma + \mathcal{G}_c\int_\Omega \gamma_d(d)\,\mathrm{d}\Omega \tag{3}$$

where $a(d) = (1-d)^2$ denotes a degradation function and $\gamma_d(d)$ represents the crack density function per unit volume. The derivation and explicit form of $\gamma_d(d)$ will be presented in Section 3.1. In Eq. (3), the integration term $\int_{\Gamma_c} p_f\,[\![\mathbf{u}\cdot\boldsymbol{n}]\!]\,\mathrm{d}\Gamma$ is still given in a discrete form (not regularised). It is difficult to carry out the integration due to unknown location of the crack opening. We will alleviate this by the phase field method in Section 3.2, where the smeared representation of $\int_{\Gamma_c} p_f\,[\![\mathbf{u}\cdot\boldsymbol{n}]\!]\,\mathrm{d}\Gamma$ will be illustrated.

2.2. Phase field regularised cohesive fracture model

Introduced in Dugdale (1960) and Barenblatt (1962) the cohesive zone model is now widely employed to model interface fracture (Xu and Needleman, 1993). The model relates tractions on a crack interface to the displacement jump along the interface. The interface Γ_c is placed in the physical domain Ω with positive and negative sides, Γ_c^+ and Γ_c^- respectively, as illustrated in Fig. 1. Tractions $\boldsymbol{p}$ are cohesive tractions $\mathbf{t}$ acting on Γ_c. In the early work, the cohesive zone model is cast in the discrete fracture model, treating the crack interface as geometric discontinuities and applying cohesive tractions on the discrete interface directly (Chen and de Borst, 2019). In the discrete model, the total energy is given as:

$$\mathcal{E}(\mathbf{u}, \Gamma; \boldsymbol{p}) = \int_\Omega \mathcal{W}(\mathbf{u})\,\mathrm{d}\Omega - \int_{\Gamma_t} \mathbf{u}\cdot\hat{\mathbf{t}}\,\mathrm{d}\Gamma + \int_\Gamma \mathcal{G}(\llbracket\mathbf{u}\rrbracket, \boldsymbol{\kappa})\,\mathrm{d}A \tag{4}$$

with $\boldsymbol{\kappa}$ being a history parameter, obeying Kuhn–Tucker conditions to distinguish between loading and unloading. $\mathcal{G}(\llbracket\mathbf{u}\rrbracket, \boldsymbol{\kappa})$ is the fracture energy function, representing the energy dissipation upon the creation of a unit crack surface. This energy is released gradually in cohesive zone models, depending on the displacement jump function $\llbracket\mathbf{u}\rrbracket$ and the history parameter $\boldsymbol{\kappa}$. The displacement jump $\llbracket\mathbf{u}\rrbracket$ across the interface Γ_c is expressed as

$$\llbracket\mathbf{u}\rrbracket = \mathbf{u}^+ - \mathbf{u}^- \qquad \text{on} \qquad \Gamma_c \tag{5}$$

with $\mathbf{u}^+$ and $\mathbf{u}^-$ being the displacement on the positive and negative sides, Γ_c^+ and Γ_c^- in Fig. 1 respectively.

The cohesive tractions are obtained by differentiating the fracture energy with respect to the displacement jump:

$$\boldsymbol{p} = \mathbf{t}(\llbracket\mathbf{u}\rrbracket, \boldsymbol{\kappa}) = \frac{\partial\mathcal{G}(\llbracket\mathbf{u}\rrbracket, \boldsymbol{\kappa})}{\partial\llbracket\mathbf{u}\rrbracket} \tag{6}$$

where $\mathbf{t}(\llbracket\mathbf{u}\rrbracket, \boldsymbol{\kappa})$ and $\llbracket\mathbf{u}\rrbracket$ are given in the global coordinate system (x_1, x_2). The traction and displacement jump in the normal and shear direction, i.e., local coordinate system (s, n) in Fig. 1, are obtained via a standard transformation:

$$\begin{aligned}\mathbf{t} &= \mathbf{R}^{\mathrm{T}}\mathbf{t}_d = \mathbf{R}^{\mathrm{T}}\left[t_s \;\; t_n\right]^{\mathrm{T}}, \qquad \llbracket\boldsymbol{v}\rrbracket = \left[\llbracket v_s\rrbracket \;\; \llbracket v_n\rrbracket\right]^{\mathrm{T}} \\ &= \mathbf{R}\llbracket\mathbf{u}\rrbracket = \mathbf{R}\left[\left\llbracket u_{x_1}\right\rrbracket \;\; \left\llbracket u_{x_2}\right\rrbracket\right]^{\mathrm{T}}\end{aligned} \tag{7}$$

with $\mathbf{R}$ being a rotation matrix (Chen et al., 2017; Chen and de Borst, 2019). The displacement jump in the normal direction $\llbracket v_n\rrbracket$ is also considered as the crack opening displacement, as defined in Eq. (2).

The cohesive fracture Γ_c can be regularised by the phase field method (Verhoosel and de Borst, 2013). In Eq. (4), the infinitesimal surface area $\mathrm{d}A$, at every point $\boldsymbol{x}_c$ on the interface Γ_c, can be rewritten in an integral form

$$\mathrm{d}A(\boldsymbol{x}_c) = \underbrace{\int_{x_n=-\infty}^{\infty}\delta(x_n)\,\mathrm{d}x_n}_{=1}\,\mathrm{d}A = \int_{x_n=-\infty}^{\infty}\delta(x_n)\,\mathrm{d}V \approx \int_{x_n=-\infty}^{\infty}\delta_c(x_n)\,\mathrm{d}V \tag{8}$$

in which $x_n = (\boldsymbol{x}-\boldsymbol{x}_c)\cdot\boldsymbol{n}(\boldsymbol{x}_c)$ and $\boldsymbol{n}(\boldsymbol{x}_c)$ the unit vector normal to the crack Γ_c. $\delta(x_n)$ represents the Dirac-delta function, being zero everywhere except at x_n. In the simulation, we cannot directly regularise the interface by using $\delta(x_n)$. An approximated form, $\delta_c(x_n)$, should be used, i.e., the last term in Eq. (8). In the current study we will employ the phase-field model to obtain $\delta_c(x_n)$. The basic idea of the phase-field model in the regularised framework is to approximate the discrete crack Γ_c by a smeared crack Γ_ξ, as shown in Fig. 1(b). The explicit form of $\delta_c(x_n)$ will be illustrated in Section 3.1. Substituting Eq. (8) into (4) leads to a phase-field regularised energy function for cohesive fracture (Verhoosel and de Borst, 2013):

$$\begin{aligned}\mathcal{E}(\mathbf{u}, \Gamma; \boldsymbol{p}) &= \int_\Omega \mathcal{W}(\mathbf{u})\,\mathrm{d}\Omega - \int_{\Gamma_t}\mathbf{u}\cdot\hat{\mathbf{t}}\,\mathrm{d}\Gamma + \int_\Gamma \mathcal{G}(\llbracket\mathbf{u}\rrbracket, \boldsymbol{\kappa})\int_{x_n=-\infty}^{\infty}\delta(x_n)\,\mathrm{d}V \\ &\approx \int_\Omega \mathcal{W}(\mathbf{u})\,\mathrm{d}\Omega - \int_{\Gamma_t}\mathbf{u}\cdot\hat{\mathbf{t}}\,\mathrm{d}\Gamma + \int_\Omega \mathcal{G}(\llbracket\mathbf{u}\rrbracket, \boldsymbol{\kappa})\,\delta_c(x_n)\,\mathrm{d}V\end{aligned} \tag{9}$$

3. Crack opening computation in the phase field method

In the variational approach to fracture, the crack geometry is not tracked explicitly (Bourdin et al., 2000). Hence the crack opening in Eqs. (2) and (7) cannot be computed directly in the regularised phase field model. Chukwudozie et al. (2019) employed an integration approach to obtain the crack opening for their analysis of hydraulic fracturing in porous media. In their analysis only brittle fracture was considered, the extension to cohesive fracture model still being open. In this section we will compute the crack opening for brittle as well as for cohesive fracture.

3.1. Smeared representation of crack

The basic idea of the phase-field model is to approximate the crack Γ_c by a smeared representation Γ_ξ, as shown in Fig. 1(b). Γ_ξ is associated with a fixed phase field $d(\mathbf{x})$ around the interface Γ_c. $d(\mathbf{x})$ equals 1 at the centre of the crack Γ_c, that is, for $x_n = 0$, and vanishes gradually away from Γ_c. The width of the smeared interface is governed by a regularisation parameter ℓ. The phase-field distribution can be determined by solving the variational problem:

$$d(\mathbf{x}) = \mathrm{Arg}\left\{\inf_{d\in S_d} \quad \Gamma_\ell(d)\right\} \tag{10}$$

in which $S_d = \left\{d \,\middle|\, d(\mathbf{x}) = 1 \;\forall\mathbf{x}\in\Gamma_c\right\}$ and

$$\Gamma_\ell(d) = \int_\Omega \gamma_d(d)\,\mathrm{d}V \tag{11}$$

where $\Gamma_\ell(d)$ denotes the crack length, i.e. the length of crack interface per unit area. $\gamma_d(d)$ represents the crack density function per unit volume. In the current study, following crack density function is employed (Chen and de Borst, 2021):

$$\gamma_d(d) = \frac{1}{\pi\ell}\left(2d(\mathbf{x}) - d(\mathbf{x})^2\right) + \frac{\ell}{\pi}\nabla d(\mathbf{x})\cdot\nabla d(\mathbf{x}), \tag{12}$$

The Euler–Lagrange equation associated with the variational equation (10) reads:

$$\begin{aligned} 1 - d(x_n) - \ell^2\frac{\mathrm{d}^2 d(x_n)}{\mathrm{d}x_n^2} = 0 \qquad & x_n \in \mathbb{R} \\ d = 1 \qquad & x_n = 0 \\ d = 0 \qquad & x_n = (-\infty, -\pi\ell/2]\bigcup[\pi\ell/2, +\infty)\end{aligned} \tag{13}$$

with the solution:

$$d(x_n) = \begin{cases} 1 - \sin\left(\dfrac{|x_n|}{\ell}\right) & -\pi\ell/2 \le x_n \le \pi\ell/2 \\ 0 & \text{otherwise}\end{cases} \tag{14}$$

with $x_n = (\boldsymbol{x}-\boldsymbol{x}_c)\cdot\boldsymbol{n}(\boldsymbol{x}_c)$, point $\boldsymbol{x}_c$ on the crack Γ_c and $\boldsymbol{n}(\boldsymbol{x}_c)$ the unit vector normal to Γ_c.

For the brittle fracture model we use Eq. (11) to compute the crack density function $\gamma_d(d)$ in Eq. (3). For the cohesive fracture model, the Dirac-delta function, $\delta_c(x_n)$ in Eq. (8), can be approximated by the crack density function in Eq. (11) (Chen and de Borst, 2022). To further simplify $\delta_c(x_n)$, we propose the following form to approximate the Dirac-delta function:

$$\begin{aligned}\delta_c(x_n) = \frac{1}{2}\left|\frac{\mathrm{d}d(x_n)}{\mathrm{d}x_n}\right| &= \frac{1}{2}\begin{cases} -\dfrac{\mathrm{d}d(x_n)}{\mathrm{d}x_n} & 0 < x_n \le \pi\ell/2 \\ \dfrac{\mathrm{d}d(x_n)}{\mathrm{d}x_n} & -\pi\ell/2 \le x_n \le 0 \\ 0 & \text{otherwise}\end{cases} \\ &= \frac{1}{2}\begin{cases}\dfrac{1}{\ell}\cos\left(\dfrac{x_n}{\ell}\right) & -\pi\ell/2 \le x_n \le \pi\ell/2 \\ 0 & \text{otherwise}\end{cases}\end{aligned} \tag{15}$$

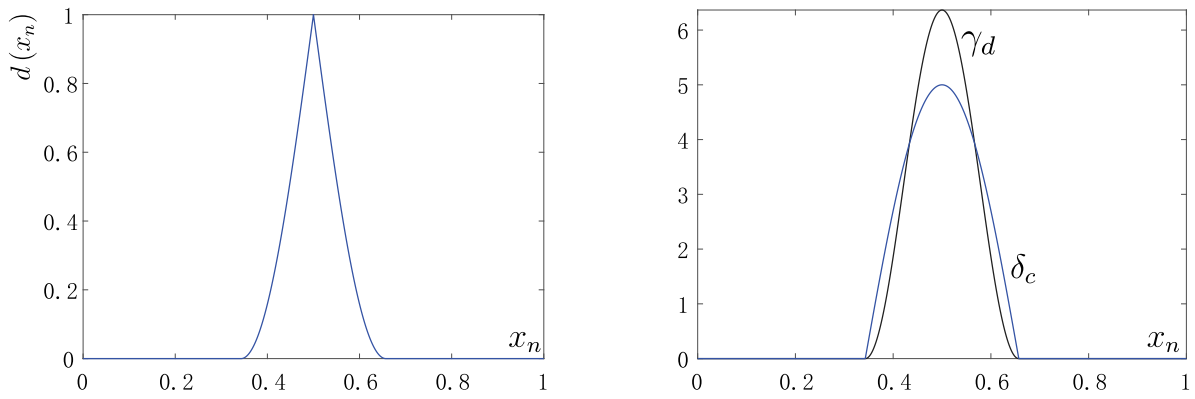

Fig. 2. One-dimensional analytical phase field $d(\mathbf{x})$, crack density function γ_c, and Dirac-delta function δ_c for a uniaxial bar (length 1) with a crack Γ_c in the middle. The regularisation length is $\ell = 0.1$.

in which the fraction $\frac{1}{2}$ stems from the constraint on the Dirac-delta function, $\int_{-\infty}^{\infty} \delta_c(x_n)\,\mathrm{d}x_n = 1$.

In Fig. 2 we plot the phase field $d(x_n)$, the crack density function $\gamma_d(d)$ and the Dirac-delta function $\delta_c(x_n)$. In the figure the distribution of $d(x_n)$, $\gamma_d(d)$ and $\delta_c(x_n)$ is localised around the crack Γ_c, confining the influence of smeared crack Γ_ξ. In Ref. Chukwudozie et al. (2019) and Yoshioka et al. (2020) the line integral of the crack opening displacement is evaluated for the range $[-\infty, \infty]$ due to the use of the AT2 phase field model. Use of the current phase-field model over the AT2 phase-field model (Chukwudozie et al., 2019; Yoshioka et al., 2020) is therefore superior.

3.2. Crack opening approximation for the brittle fracture

The term $\int_{\Gamma_c} p_f\,[\![\mathbf{u}\cdot\boldsymbol{n}]\!]\,\mathrm{d}\Gamma$ in the brittle fracture model, i.e., in Eq. (3), has a discrete format, i.e., is not regularised. Chukwudozie et al. (2019) have proposed the following smeared approximation:

$$\int_{\Gamma_c} p_f\,[\![\mathbf{u}\cdot\boldsymbol{n}]\!]\,\mathrm{d}\Gamma \approx -\int_{\Omega} p_f\,\mathbf{u}\cdot\nabla d\,\mathrm{d}\Omega \tag{16}$$

where the minus sign in front of the integration originates from the definition of the phase-field variable d, being different from that in Chukwudozie et al. (2019).

The profile of phase-field variable d in the direction normal to Γ_c is given in Eq. (14). Integrating the phase field gradient in the normal direction $\boldsymbol{n}$, we arrive at:

$$\int_{-\infty}^{0} \left|\nabla d\,(x_n)\right| \mathrm{d}x_n = \int_{0}^{\infty} \left|\nabla d\,(x_n)\right| \mathrm{d}x_n = 1 \tag{17}$$

The crack opening displacement Γ_c then reads:

$$\begin{aligned}[\![\mathbf{u}\cdot\boldsymbol{n}]\!] &= \mathbf{u}\left(x_n^+\right)\cdot\boldsymbol{n} - \mathbf{u}\left(x_n^-\right)\cdot\boldsymbol{n} = \mathbf{u}\left(x_n^+\right)\cdot\boldsymbol{n}\int_0^{\infty}\left|\nabla d\,(x_n)\right|\mathrm{d}x_n \\ &\quad - \mathbf{u}\left(x_n^-\right)\cdot\boldsymbol{n}\int_{-\infty}^{0}\left|\nabla d\,(x_n)\right|\mathrm{d}x_n\end{aligned} \tag{18}$$

with x_n^+ and x_n^- being points on positive and negative sides of the crack Γ_c, i.e., Γ_c+ and Γ_c- in Fig. 1(a) respectively.

Due to the compact support of the phase-field model, as illustrated in Fig. 2, the displacements $\mathbf{u}\left(x_n^+\right)$ and $\mathbf{u}\left(x_n^-\right)$ can be considered as constants in the direction normal to the crack, yielding:

$$\begin{aligned}\mathbf{u}\left(x_n^+\right)\cdot\boldsymbol{n}\int_0^{\infty}\left|\nabla d\,(x_n)\right|\mathrm{d}x_n &\approx \int_0^{\infty}\mathbf{u}\,(x_n)\cdot\boldsymbol{n}\left|\nabla d\,(x_n)\right|\mathrm{d}x_n \\ \mathbf{u}\left(x_n^-\right)\cdot\boldsymbol{n}\int_{-\infty}^{0}\left|\nabla d\,(x_n)\right|\mathrm{d}x_n &\approx \int_{-\infty}^{0}\mathbf{u}\,(x_n)\cdot\boldsymbol{n}\left|\nabla d\,(x_n)\right|\mathrm{d}x_n\end{aligned} \tag{19}$$

The normal vector $\boldsymbol{n}$ can subsequently be approximated as (Chukwudozie et al., 2019):

$$\boldsymbol{n} \approx -\nabla d\left(x_n^+\right) \Big/ \left|\nabla d\left(x_n^+\right)\right| \approx \nabla d\left(x_n^-\right) \Big/ \left|\nabla d\left(x_n^-\right)\right| \tag{20}$$

Substituting Eq. (20) into (18) and employing Eq. (19) we obtain the crack opening displacement for the brittle fracture model, as follows:

$$[\![\mathbf{u}\cdot\boldsymbol{n}]\!] = \mathbf{u}\left(x_n^+\right)\cdot\boldsymbol{n} - \mathbf{u}\left(x_n^-\right)\cdot\boldsymbol{n} \approx -\int_{-\infty}^{\infty}\mathbf{u}\,(x_n)\cdot\nabla d\,(x_n)\,\mathrm{d}x_n \tag{21}$$

which can be simplified as

$$[\![\mathbf{u}\cdot\boldsymbol{n}]\!] = \mathbf{u}\left(x_n^+\right)\cdot\boldsymbol{n} - \mathbf{u}\left(x_n^-\right)\cdot\boldsymbol{n} \approx -\int_{-\pi\ell/2}^{\pi\ell/2}\mathbf{u}\,(x_n)\cdot\nabla d\,(x_n)\,\mathrm{d}x_n \tag{22}$$

where the phase field model in Eqs. (13) and (14) is considered.

3.3. Crack opening approximation for the cohesive fracture

Following the concept of a smeared area in Eq. (8), In the cohesive fracture model we can regularise the displacement jump function using the Dirac-delta function:

$$[\![\mathbf{u}]\!](\boldsymbol{x}_c) = \int_{x_n=-\infty}^{\infty}\boldsymbol{v}(\boldsymbol{x})\,\delta(x_n)\,\mathrm{d}x_n \approx \int_{x_n=-\infty}^{\infty}\boldsymbol{v}(\boldsymbol{x})\,\delta_c(x_n)\,\mathrm{d}x_n \tag{23}$$

with $x_n = (\boldsymbol{x}-\boldsymbol{x}_c)\cdot\boldsymbol{n}(\boldsymbol{x}_c)$ and $\boldsymbol{n}(\boldsymbol{x}_c)$ the unit vector normal to the crack Γ_c. $\boldsymbol{v}(\boldsymbol{x})$ is an auxiliary field employed to approximate the displacement jump in a smeared sense (Chen and de Borst, 2022). Employing the variational principle for minimising $\mathcal{E}(\mathbf{u}, \Gamma; \boldsymbol{p})$ in Eq. (9) with respect to the displacement $\mathbf{u}$ and the auxiliary field $\boldsymbol{v}$, we obtain the weak form of the cohesive fracture problem (Verhoosel and de Borst, 2013; Chen and de Borst, 2022). Applying the divergence theorem to the weak form equation yields the elastic strain $\boldsymbol{\varepsilon}^e$ (Verhoosel and de Borst, 2013):

$$\varepsilon_{ij}^e = u_{(i,j)} - \mathrm{sym}\left(v_i n_j\right)\delta_c \tag{24}$$

with n_j being the component of the unit vector normal to the interface Γ_c. Obviously, the 'elastic' strain $\boldsymbol{\varepsilon}^e$ is composed of the gradient of the displacement and the term related to the displacement jump. In deriving Eq. (24), the variational principle has been employed.

Alternatively, the extended finite element method (XFEM) can be used to arrive at Eq. (24) (Chen and de Borst, 2022). In XFEM the displacement function is composed of a continuous part, $\mathbf{w}(\boldsymbol{x})$, and a bounded part that modulates the displacement jump over the domain through the Heaviside function $\mathscr{H}$ (Khoei, 2014):

$$\mathbf{u}(\boldsymbol{x}) = \mathbf{w}(\boldsymbol{x}) + \mathscr{H}(\boldsymbol{x})\,\boldsymbol{v}(\boldsymbol{x}) \tag{25}$$

with $\boldsymbol{v}(\boldsymbol{x})$ being the displacement jump. The Heaviside function $\mathscr{H}$ is here defined as:

$$\mathscr{H}(\boldsymbol{x}) = \frac{1}{2}\begin{cases}1 - d\,(x_n) & \text{if} \quad \boldsymbol{x}\in\Omega^+ \\ d\,(x_n) - 1 & \text{otherwise}\end{cases} \tag{26}$$

with Ω^+ being the domain at the positive side of the interface Γ_c^+. $d\,(x_n)$ denotes the phase field function.

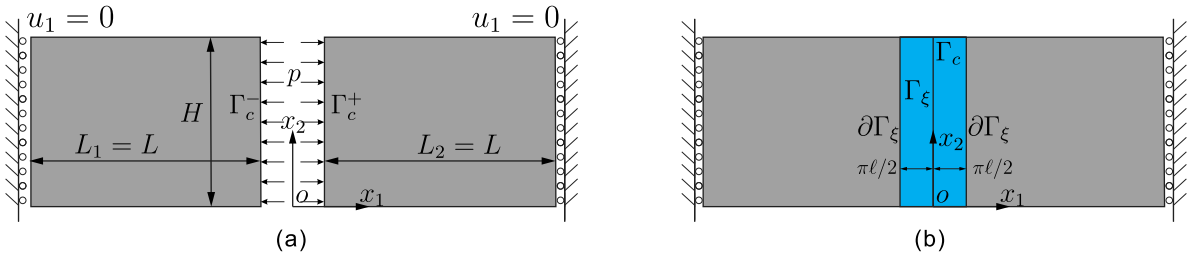

Fig. 3. (a) uniaxial compression of a bar with a crack Γ_c; (b) smeared crack Γ_ξ (blue area). Here a constant pressure p is applied in the crack Γ_c, exerted on positive and negative sides, Γ_c^+ and Γ_c^-, respectively.

Employing the phase-field model in Eq. (14), we obtain the following form of the Heaviside function $\mathscr{H}$

$$\mathscr{H}(\boldsymbol{x}) = \frac{1}{2}\begin{cases} 1 & \pi\ell/2 \le x_n \\ \sin\left(\dfrac{x_n}{\ell}\right) & -\pi\ell/2 \le x_n \le \pi\ell/2 \\ -1 & \text{otherwise} \end{cases} \tag{27}$$

Considering the small strain assumption, the infinitesimal strain field becomes (Fathi et al., 2021; Chen et al., 2022)

$$\varepsilon_{ij} = u_{(i,j)} = \mathrm{w}_{(i,j)} + \mathscr{H} v_{(i,j)} + \mathrm{sym}\left(v_i n_j\right)\delta_c \tag{28}$$

with δ_c being the Dirac-delta function. In this way we can arrive at the 'elastic' strain Eq. (24) by taking the form:

$$\varepsilon^e_{ij} = u_{(i,j)} - \varepsilon^\rho_{ij} \quad \Rightarrow \quad \varepsilon^e_{ij} = \mathrm{w}_{(i,j)} + \mathscr{H} v_{(i,j)} \quad \text{and} \quad \mathrm{sym}\left(v_i n_j\right)\delta_c = \varepsilon^\rho_{ij} \tag{29}$$

Obviously, the elastic strain as derived in Eq. (24) is identical to that in the regularised extended finite element method. Accordingly, the displacement field $\mathbf{u}$ in the cohesive fracture model, i.e., Eq. (9), can be written in the form of Eq. (25).

If we multiply Eq. (25) with the normal vector $\boldsymbol{n}$, defined in Eq. (20), and integrate over the normal direction $x_n \in [-\infty\ \infty]$, we obtain an approximated form of the crack opening displacement for the cohesive fracture model:

$$[\![\mathbf{u}\cdot\boldsymbol{n}]\!] = \boldsymbol{v}(\boldsymbol{x})\cdot\boldsymbol{n} \approx -2\int_{-\infty}^{\infty} \mathbf{u}\left(x_n\right)\cdot\nabla d\left(x_n\right)\mathrm{d}x_n \tag{30}$$

where Eq. (17) has been used.

Eq. (30) can be simplified if we consider the phase-field model in Eq. (14):

$$[\![\mathbf{u}\cdot\boldsymbol{n}]\!] = \boldsymbol{v}(\boldsymbol{x})\cdot\boldsymbol{n} \approx -2\int_{-\pi\ell/2}^{\pi\ell/2} \mathbf{u}\left(x_n\right)\cdot\nabla d\left(x_n\right)\mathrm{d}x_n \tag{31}$$

where the factor '2' in front of the integration stems from the fraction $\frac{1}{2}$ in Eq. (26). Eq. (30) presents an integral form of the crack opening displacement along the cohesive crack Γ_c. It can directly be used in the cohesive fracture model, i.e., Eq. (9).

4. Validation of the computation of the crack opening displacement

To validate the proposed formulations for the crack opening displacement computation, we will consider a two-dimensional version of a uniaxial compression problem, as illustrated in Fig. 3(a). The Young's modulus of the plate is E. A crack is defined at $x_1 = 0$ and a constant pressure, p, is applied in the crack. Due to the set-up of the problem, only mode-I crack opening is included in the analysis. The crack is regularised by the phase-field variable over the regularisation zone $\left(-\pi\ell/2 \le x_1 \le \pi\ell/2\right)$, as shown in Fig. 3(b). The analytical solution of the displacement, of the crack opening displacement and of the stress reads:

$$u_1\left(x_1, x_2\right) = \begin{cases} p_s\left(L - x_1\right) & 0 < x_1 \\ -p_s\left(L + x_1\right) & x_1 < 0 \end{cases}$$
$$[\![\mathbf{u}\cdot\boldsymbol{n}]\!] = 2p_s L \qquad \sigma_1\left(x_1, x_2\right) = -p \tag{32}$$

with $p_s = p/E$. The factor '2' in front of $[\![\mathbf{u}\cdot\boldsymbol{n}]\!]$ stems from the symmetric crack opening about the vertical axis.

Next we will solve the problem in the framework of phase-field modelling. We will separately consider the pressure p as a fluid pressure in the brittle fracture model, and a constant cohesive traction (independent of the crack opening) in the cohesive fracture model.

4.1. Brittle fracture solution

Substituting Eq. (16) into (3) leads to a smeared form of the energy functional:

$$\mathcal{E}(\mathbf{u}, \Gamma; \boldsymbol{p}) = \int_\Omega a(d)\,\mathcal{W}(\mathbf{u})\,\mathrm{d}\Omega - \int_{\Gamma_t} \mathbf{u}\cdot\hat{\mathbf{t}}\,\mathrm{d}\Gamma + \int_\Omega p_f \mathbf{u}\cdot\nabla d\,\mathrm{d}\Omega + \mathcal{G}_c\int_\Omega \gamma_d(d)\,\mathrm{d}\Omega \tag{33}$$

For the problem given in Fig. 3 we obtain the momentum balance equation from the variational principle of Eq. (33):

$$\begin{aligned} \frac{\mathrm{d}}{\mathrm{d}x_1}\left(\left(1 - d\left(x_1\right)\right)^2 \frac{\mathrm{d}u_1}{\mathrm{d}x_1}\right) - p_s\frac{\mathrm{d}}{\mathrm{d}x_1}d\left(x_1\right) = 0 \qquad & -\pi\ell/2 \le x_1 \le \pi\ell/2 \\ \frac{\mathrm{d}}{\mathrm{d}x_1}\left(\frac{\mathrm{d}u_1}{\mathrm{d}x_1}\right) = 0 \qquad & \text{otherwise} \end{aligned} \tag{34}$$

with the phase field $d\left(x_1\right)$ given as

$$d\left(x_1\right) = 1 - \sin\left(\frac{|x_1|}{\ell}\right) \qquad -\pi\ell/2 \le x_1 \le \pi\ell/2 \tag{35}$$

Considering the boundary condition of $u_1 = 0$ at $x_1 = \pm L$, and the continuous displacement at $x_1 = \pm\pi\ell/2$, we obtain the displacement:

$$u_1\left(x_1, x_2\right) = \begin{cases} p_s\left(L - x_1\right) & \pi\ell/2 \le x_1 \le L \\ -p_s\ell\ln\left(\left|\tan\left(\dfrac{x_1}{2\ell}\right)\right|\right) + p_s\left(L - \dfrac{\pi\ell}{2}\right) & 0 < x_1 \le \pi\ell/2 \\ p_s\ell\ln\left(\left|\tan\left(\dfrac{x_1}{2\ell}\right)\right|\right) - p_s\left(L - \dfrac{\pi\ell}{2}\right) & -\pi\ell/2 \le x_1 < 0 \\ -p_s\left(L + x_1\right) & -L \le x_1 \le -\pi\ell/2 \end{cases} \tag{36}$$

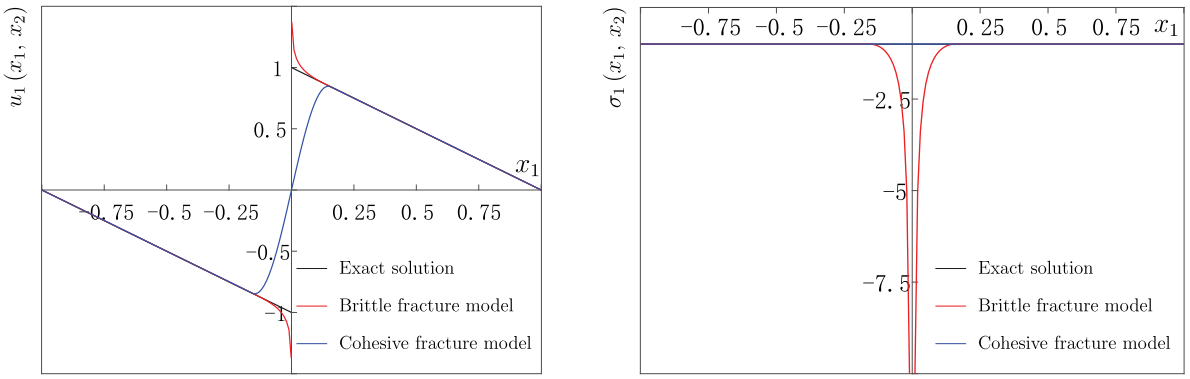

Fig. 4. Displacement u_1 and stress σ_1 for the uniaxial bar in Fig. 3(a). The length of the bar is $L = 1$ and the regularisation length is $\ell = 0.1$.

which yields the stress $\sigma_1(x_1, x_2)$:

$$\sigma_1(x_1, x_2) = \begin{cases} -p\csc\left(\frac{x_1}{\ell}\right) & 0 < x_1 \le \pi\ell/2 \\ p\csc\left(\frac{x_1}{\ell}\right) & -\pi\ell/2 \le x_1 < 0 \\ -p & \text{otherwise} \end{cases} \tag{37}$$

Fig. 4 gives the comparison between phase-field solutions and the analytical solution. For the brittle fracture model, the displacement and the stress lead to infinite values at the crack Γ_c due to the term $\ln\left(\left|\tan\left(\frac{x_1}{2\ell}\right)\right|\right)$ in Eq. (36). The displacement shows an obvious jump at Γ_c due to the brittle feature of the crack. The solutions tend to the analytical solution when x_1 approaches the boundary of the phase-field profile, i.e. $x_1 \to \pm\pi\ell/2$.

The crack opening displacement of the plate is obtained by Eq. (22):

$$\begin{aligned}
[\![\mathbf{u}\cdot\boldsymbol{n}]\!] &\approx -\int_{-\pi\ell/2}^{\pi\ell/2} u(x_1, x_2)\cdot\frac{\mathrm{d}d(x_1)}{\mathrm{d}x_1}\mathrm{d}x_1 \\
&= -\int_{-\pi\ell/2}^{0^-}\left(p_s\ell\ln\left(\left|\tan\left(\frac{x_1}{2\ell}\right)\right|\right)\right. \\
&\left.-p_s\left(L-\frac{\pi\ell}{2}\right)\right)\frac{1}{\ell}\cos\left(\frac{x_1}{\ell}\right)\mathrm{d}x_1 \\
&\quad -\int_{0^+}^{\pi\ell/2}\left(p_s\ell\ln\left(\left|\tan\left(\frac{x_1}{2\ell}\right)\right|\right)\right. \\
&\left.-p_s\left(L-\frac{\pi\ell}{2}\right)\right)\frac{1}{\ell}\cos\left(\frac{x_1}{\ell}\right)\mathrm{d}x_1 \\
&= -\int_{-\pi\ell/2}^{0^-} p_s\ell\ln\left(\left|\tan\left(\frac{x_1}{2\ell}\right)\right|\right)\frac{1}{\ell}\cos\left(\frac{x_1}{\ell}\right)\mathrm{d}x_1 \\
&\quad -\int_{0^+}^{\pi\ell/2} p_s\ell\ln\left(\left|\tan\left(\frac{x_1}{2\ell}\right)\right|\right)\frac{1}{\ell}\cos\left(\frac{x_1}{\ell}\right)\mathrm{d}x_1 \\
&\quad +\int_{-\pi\ell/2}^{\pi\ell/2} p_s\left(L-\frac{\pi\ell}{2}\right)\frac{1}{\ell}\cos\left(\frac{x_1}{\ell}\right)\mathrm{d}x_1 \\
&= -2\int_{0^+}^{\pi\ell/2} p_s\ell\ln\left(\left|\tan\left(\frac{x_1}{2\ell}\right)\right|\right)\frac{1}{\ell}\cos\left(\frac{x_1}{\ell}\right)\mathrm{d}x_1 \\
&\quad +\int_{-\pi\ell/2}^{\pi\ell/2} p_s\left(L-\frac{\pi\ell}{2}\right)\frac{1}{\ell}\cos\left(\frac{x_1}{\ell}\right)\mathrm{d}x_1
\end{aligned} \tag{38}$$

The integration of the first part in Eq. (38) yields

$$\begin{aligned}
&-2\int_{0^+}^{\pi\ell/2} p_s\ell\ln\left(\left|\tan\left(\frac{x_1}{2\ell}\right)\right|\right)\frac{1}{\ell}\cos\left(\frac{x_1}{\ell}\right)\mathrm{d}x_1 \\
&= -2p_s\ell\left[\ln\left(\tan\left(\frac{x_1}{2\ell}\right)\right)\sin\left(\frac{x_1}{\ell}\right)-\frac{1}{\ell}x_1\right]_{0^+}^{\pi\ell/2}
\end{aligned} \tag{39}$$

Employing L'Hospital's rule we can solve the integral of Eq. (39):

$$-2\int_{0^+}^{\pi\ell/2} p_s\ell\ln\left(\left|\tan\left(\frac{x_1}{2\ell}\right)\right|\right)\frac{1}{\ell}\cos\left(\frac{x_1}{\ell}\right)\mathrm{d}x_1 = \pi p_s\ell \tag{40}$$

which leads to the crack opening displacement for the brittle fracture model:

$$\begin{aligned}
[\![\mathbf{u}\cdot\boldsymbol{n}]\!] &= -2\int_{0^+}^{\pi\ell/2} p_s\ell\ln\left(\left|\tan\left(\frac{x_1}{2\ell}\right)\right|\right)\frac{1}{\ell}\cos\left(\frac{x_1}{\ell}\right)\mathrm{d}x_1 \\
&\quad +\int_{-\pi\ell/2}^{\pi\ell/2} p_s\left(L-\frac{\pi\ell}{2}\right)\frac{1}{\ell}\cos\left(\frac{x_1}{\ell}\right)\mathrm{d}x_1 \\
&= \pi p_s\ell + 2p_s\left(L-\frac{\pi\ell}{2}\right) = 2p_sL
\end{aligned} \tag{41}$$

being identical to the analytical solution in Eq. (32).

4.2. Cohesive fracture solution

For the phase-field regularised cohesive fracture model we depart from the strain in Eq. (24). For the problem stated in Fig. 3 we then get the stress from the Hooke's law:

$$\sigma_1(x_1, x_2) = E\left(\frac{\mathrm{d}}{\mathrm{d}x_1}u_1(x_1, x_2) - \delta_c v\right) \tag{42}$$

with v being the crack opening displacement; δ_c being Dirac-delta function defined in Eq. (15). The momentum balance equation reads

$$\sigma_1(x_1, x_2) = E\left(\frac{\mathrm{d}}{\mathrm{d}x_1}u_1(x_1, x_2) - \delta_c v\right) = -p \tag{43}$$

which is equal to the analytical solution of $\sigma_1(x_1, x_2)$ in Eq. (32).

Remark. Eqs. (42) and (43) consider the case of uniaxial deformation of a bar with a straight crack Γ_c. Γ_c is regularised as a smeared crack Γ_ξ by the Dirac-delta function δ_c, see Fig. 3(b). Even though Fig. 3 presents a two-dimensional fracture problem, it still represents uniaxial deformation. The crack Γ_c is a straight crack in the domain and is perpendicular to the axis of the uniaxial bar, here the horizontal axis x_1 in Fig. 3(a). Thus, the analysis in Section 4.2 is restricted to the phase-field model which induces a straight crack, perpendicular to the bar axis. Indeed, if the phase-field model with an anisotropic fracture constitutive law would produce a straight crack, perpendicular to the bar axis, the method in this section could be used to compute the crack opening displacement.

Considering the boundary conditions of $u_1 = 0$ at $x_1 = \pm L$, and the continuous displacement field at $x_1 = \pm\pi\ell/2$, we can derive the displacement as:

$$u_1(x_1, x_2) = \begin{cases} p_s(L - x_1) & \pi\ell/2 \le x_1 \le L \\ \frac{v}{2}\sin\left(\frac{x_1}{\ell}\right) - p_s x_1 & -\pi\ell/2 < x_1 \le \pi\ell/2 \\ -p_s(L + x_1) & -L \le x_1 \le -\pi\ell/2 \end{cases} \tag{44}$$

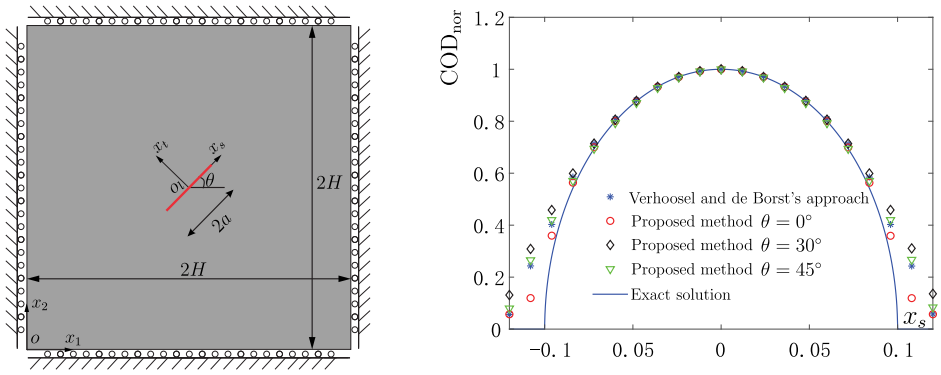

(a) geometry and boundary conditions (b) normalised crack opening displacement

Fig. 5. (a) 2D inclined line crack ($x_s = -a$ to $x_s = a$) with a the half length under a constant pressure p. The crack is represented by the red line. The inclination angle of the crack is θ. (x_1, x_2) is the global coordinate with the origin O, while (x_s, x_t) is the local coordinate along the crack; (b) normalised crack opening displacement for different values of the inclination angle θ. The normalised crack opening displacement is defined as $\mathrm{COD}_{\mathrm{nor}} = \mathrm{COD}/\mathrm{COD}^{\mathrm{m}}_{\mathrm{ana}}$, where $\mathrm{COD}^{\mathrm{m}}_{\mathrm{ana}}$ is the exact solution of the maximum crack opening displacement (Eq. (49)), being at the origin O_t in the current study. For brevity, we only present the results of Verhoosel and de Borst's approach for $\theta = 0°$.

Fig. 4 presents the comparison between phase-field solutions and the analytical solution. For the cohesive fracture model, the displacement shows some discrepancies in the range of the smeared crack Γ_ξ (as illustrated in Fig. 3(b)), due to the regularised interface. The displacement is continuous along the bar due to the continuous Dirac-delta function definition in Eq. (15). In Fig. 4(b), the stress σ_1 is consistent with the analytical solution.

We now can compute the crack opening displacement from the integration Eq. (31):

$$\begin{aligned}
[\![\mathbf{u}\cdot\boldsymbol{n}]\!] = \upsilon &\approx -2\int_{-\pi\ell/2}^{\pi\ell/2} u\left(x_1, x_2\right)\cdot\frac{\mathrm{d}d\left(x_1\right)}{\mathrm{d}x_1}\mathrm{d}x_1 \\
&= -2\int_{-\pi\ell/2}^{0}\left(\frac{\upsilon}{2}\sin\left(\frac{x_1}{\ell}\right) - p_s x_1\right)\frac{1}{\ell}\cos\left(\frac{x_1}{\ell}\right)\mathrm{d}x_1 \\
&+ 2\int_{0}^{\pi\ell/2}\left(\frac{\upsilon}{2}\sin\left(\frac{x_1}{\ell}\right) - p_s x_1\right)\frac{1}{\ell}\cos\left(\frac{x_1}{\ell}\right)\mathrm{d}x_1 \\
&= 4\int_{0}^{\pi\ell/2}\left(\frac{\upsilon}{2}\sin\left(\frac{x_1}{\ell}\right) - p_s x_1\right)\frac{1}{\ell}\cos\left(\frac{x_1}{\ell}\right)\mathrm{d}x_1 \\
&= \upsilon + 2p_s\ell\left(\pi - 2\right)
\end{aligned} \tag{45}$$

obviously, this solution leads to the exact crack opening displacement when $\ell \to 0$.

Until now, the crack opening displacement υ is unknown. Herein, we obtain the crack opening displacement υ from the continuity condition at $x_1 = \pm\pi\ell/2$:

$$\upsilon = 2p_s L \tag{46}$$

which result is identical to the analytical solution in Eq. (32). Substituting Eq. (46) into Eq. (45) and considering the limiting case when $\ell \to 0$ we obtain the crack opening displacement in an explicit format:

$$[\![\mathbf{u}\cdot\boldsymbol{n}]\!] = \lim_{\ell\to 0}\left(\upsilon + 2p_s\ell\left(\pi - 2\right)\right) = \upsilon = 2p_s L \tag{47}$$

In sum, for the same problem, the brittle and cohesive fracture model will lead to different solutions of the displacement and stress. The displacement of the brittle fracture model shows a jump at the crack, while that of the cohesive interface model is continuous. For the stress, the brittle fracture model yields an infinite value, while the cohesive model is consistent with analytical solution. Also the displacement and the stress of the brittle fracture model are different from those of the cohesive fracture model, but both models lead to an identical crack opening displacement, thus validating the proposed formulations.

5. Numerical example

We now demonstrate the performance of the methodology to compute the crack opening displacement in a multi-dimensional setting through two representative examples. First, we will consider an infinite plate with a pressurised internal crack. Then, a fibre–epoxy debonding test is considered to explore cohesive interface debonding under mixed-mode loading conditions, showing the ability of the method to analyse curved cracks. To well represent the crack in a smeared sense, the regularisation length is always chosen as $l \geq 4h$ (h: element size around the crack) (Bourdin et al., 2008).

We employ Eqs. (22) and (31) to compute the crack opening displacement, depending on the fracture model, i.e., brittle or cohesive fracture. For brittle fracture Eq. (3) has been validated by comparing numerical results with the closed-form solution of Eq. (21) (Wheeler et al., 2014; Chukwudozie et al., 2019; Yoshioka et al., 2020) and will not be discussed here. The cohesive phase-field model, i.e., Eq. (9), includes the displacement $\mathbf{u}$ and the displacement jump $[\![\mathbf{u}]\!]$ as variables. In the phase-field model the crack is represented in a smeared format, Γ_ξ, see Fig. 1(b), and the displacement jump cannot be computed directly due to unknown displacement jump location (Chukwudozie et al., 2019). To solve this issue Verhoosel and de Borst (2013) have proposed a cohesive phase-field model, which uses an auxiliary field $\boldsymbol{\upsilon}$ to model the displacement jump $[\![\mathbf{u}]\!]$, required as input in a cohesive-zone model, see also Vignollet et al. (2014), May et al. (2015), Ghaffari Motlagh and de Borst (2020) and Chen and de Borst (2022). To describe the interface behaviour the cohesive zone law from the discrete model is used directly (Chen and de Borst, 2022). Obviously, in Verhoosel and de Borst's approach, the displacement jump, including the crack opening displacement and the displacement jump in the shear direction, can be obtained directly from the finite element solution of system equations (Chen and de Borst, 2022). Hence, for the first example, we will also use this solution of the crack opening displacement as an additional reference solution, next to the closed form solution. Herein, we will obtain the displacement $\mathbf{u}$, and then use Eq. (30) to compute the crack opening displacement, in order to validate the proposed approach in Section 3.3.

In the numerical solution we exploit C^1-continuous Powell–Sabin B-splines, which are based on triangles, for the spatial discretisation (Chen and de Borst, 2019; Chen et al., 2020). A flexible control

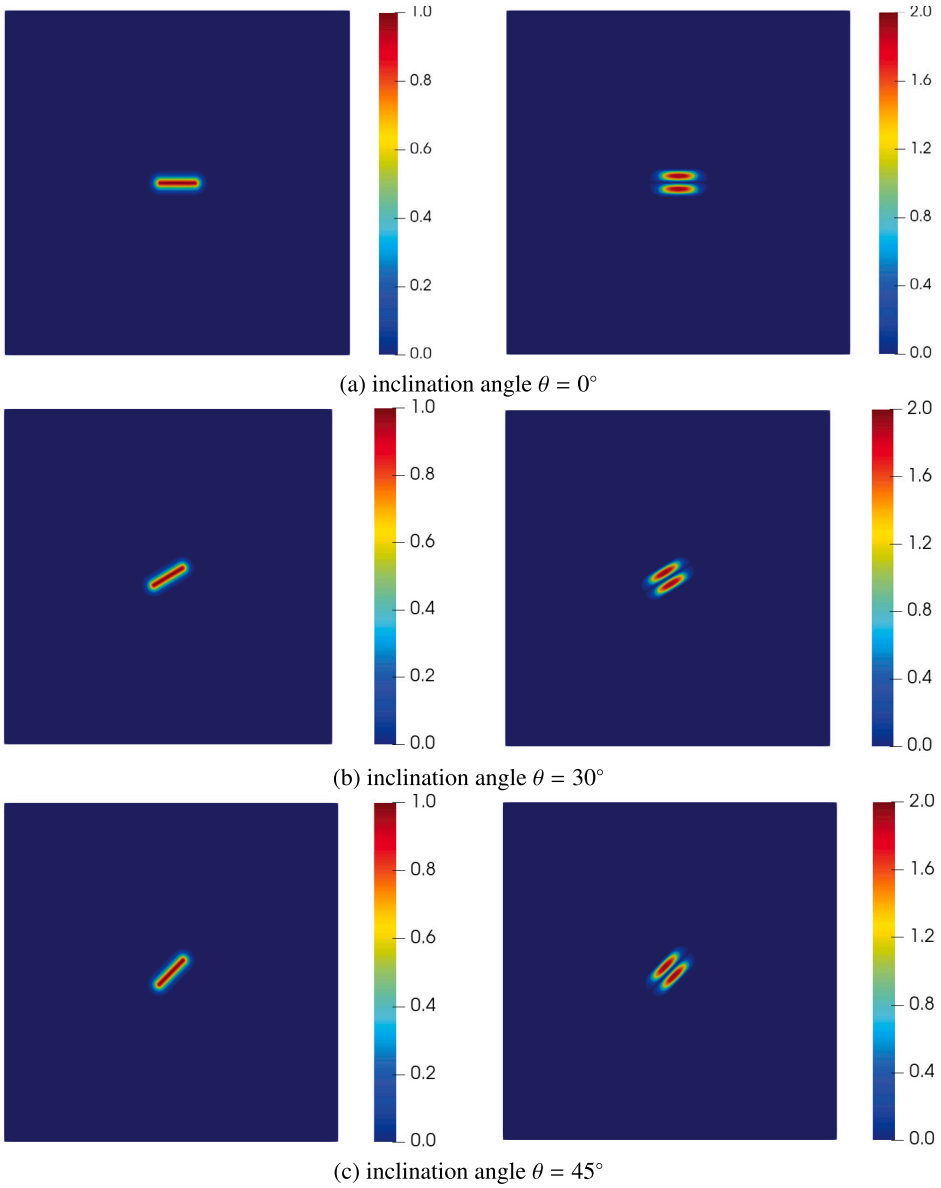

(a) inclination angle $\theta = 0°$

(b) inclination angle $\theta = 30°$

(c) inclination angle $\theta = 45°$

Fig. 6. Plot of the phase field d and $\mathbf{u} \cdot \nabla d$ for different values of the inclination angle θ. The figures in the left column represent the phase field d, while the figures in the right column denote $\mathbf{u} \cdot \nabla d$.

of the geometry is possible, such as remeshing using any standard package for triangular elements (Geuzaine and Remacle, 2009), while the C^1-continuity assures an improved stress prediction (Chen et al., 2019). The plate has been discretised by the triangulation presented in Fig. 5(b). Powell–Sabin B-splines describe the geometry and interpolate the displacement field $\mathbf{u}$ and the displacement jump $\boldsymbol{v}$ in an isoparametric sense (Chen and de Borst, 2019):

$$\boldsymbol{x} = \sum_{k=1}^{N_v} \sum_{j=1}^{3} N_k^j \boldsymbol{X}_k^j = \boldsymbol{N}\boldsymbol{X} \qquad \mathbf{u} = \sum_{k=1}^{N_v} \sum_{j=1}^{3} N_k^j \boldsymbol{U}_k^j = \boldsymbol{N}\boldsymbol{U}$$
$$\boldsymbol{v} = \sum_{k=1}^{N_v} \sum_{j=1}^{3} N_k^j \boldsymbol{\vartheta}_k^j = \boldsymbol{N}\boldsymbol{\vartheta}, \tag{48}$$

where $\boldsymbol{X}_k^j$ represent the coordinates of the corners $\boldsymbol{Q}_k^j$ of the Powell–Sabin triangles, $\boldsymbol{U}_k^j$ and $\boldsymbol{\vartheta}_k^j$ denote the degrees of freedom at $\boldsymbol{Q}_k^j$, and N_v is the total number of vertices. The indices $j = 1, 2, 3$ imply that three Powell–Sabin B-splines N_k^j are defined on each vertex k. $\boldsymbol{N}$, $\boldsymbol{X}$, $\boldsymbol{U}$ and $\boldsymbol{\vartheta}$ are the shape function matrix, the vector of the coordinates, the displacement, the displacement jump, respectively.

5.1. Infinite plate with a pressurised internal crack

We consider an infinite domain Ω with an inclined internal crack Γ (length $2a$), as illustrated in Fig. 5(a). The inclination angle of the crack is θ. The crack surface is pressurised by a constant pressure p. For this problem an exact solution can be obtained under the assumption that the displacement and stress vanish at infinity (Sneddon and Lowengrub, 1969). The closed-form solution for the crack opening displacement (COD) is given by:

$$\text{COD} = [\![\mathbf{u} \cdot \boldsymbol{n}]\!] = \frac{4pa}{E'} \sqrt{\left(1 - \frac{x_s^2}{a^2}\right)} \tag{49}$$

with $E' = E/\left(1 - \nu^2\right)$ where E and ν are Young's modulus and Poisson's ratio, respectively. $\left(x_s, x_t\right)$ is the local coordinate along the

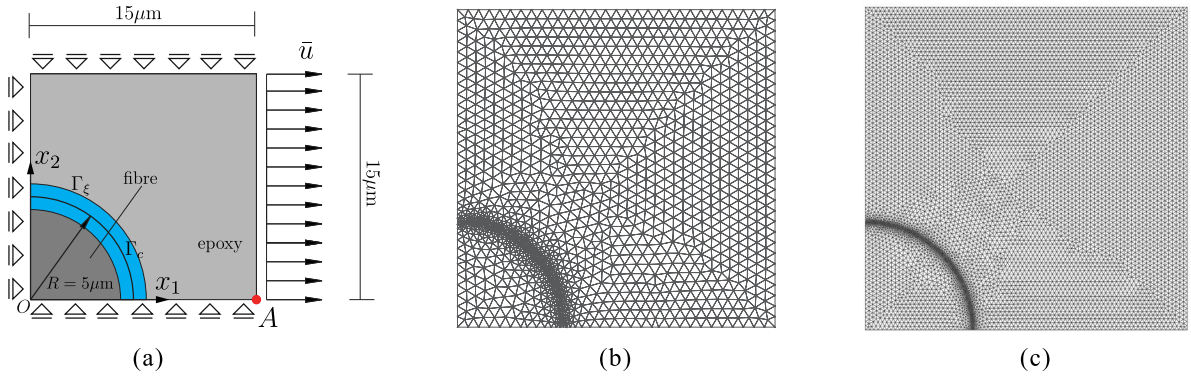

Fig. 7. (a) geometry and boundary conditions of one quarter of the fibre (Chen and de Borst, 2022), where the blue area indicates the smeared interface Γ_ξ; (b) domain triangulation with the smallest element size $e = 0.10$; (c) domain triangulation with the smallest element size $e = 0.04$. In the figure, the blue area represents the smeared interface Γ_ξ. To well describe Γ_ξ, the mesh around the interface Γ_c is refined with the smallest element size e. A discrete interface model is employed to provide the reference solution.

crack. The origin is set at the centre of the crack O_l. In addition to the analytical solution, the numerical solution of Verhoosel and de Borst (2013) has been used for validation of the present method.

In the simulation the size of the domain has been chosen such that the influence of boundary condition $\partial\Omega$ on the displacement field near the crack almost vanishes. A square domain $\Omega = [-1, 1] \times [-1, 1]$ has been used to this end. The centre of the crack is at $(x_1, x_2) = (0, 0)$. The half crack length $a = 0.1$. With a suitable re-scaling of the loading the material properties can be chosen as: Young's modulus $E = 1$ and Poisson's ratio $\nu = 0.1$. The regularisation length is set $\ell = 0.05$. The traction on the crack surface is chosen as $p = 1$.

We consider three values of the inclination angle, $\theta = 0°$, $30°$ and $45°$, respectively. The profiles of the phase field and of $\mathbf{u}\cdot\nabla d$ are shown in Fig. 6. $\mathbf{u}\cdot\nabla d$ results from the post-processing of the solution of cohesive phase-field model. The plots of the phase field and of $\mathbf{u}\cdot\nabla d$ are confined to a local area around the crack, due to the narrow distribution of the phase field, as illustrated in Fig. 2. Both d and $\mathbf{u}\cdot\nabla d$ show nearly identical profiles for the different values of the inclination angle θ.

Next, a line integral of $-2\mathbf{u}\cdot\nabla d$ is taken in the direction normal to the crack. The limit of the integration is $\left[-\pi\ell/2, \pi\ell/2\right]$, because of the definition of the phase field in Eq. (14). The line integral is evaluated numerically by Gaussian quadrature. For this problem, the crack opening displacement (COD) should be identical no matter the choice of θ. In Fig. 5(b) the results are compared with the closed form solution in Eq. (49) and for $\theta = 0°$ also with the numerical solution of Verhoosel and de Borst (2013). Invariably, the results match very well.

5.2. Fibre–epoxy debonding test

To demonstrate the ability of the method to analyse curved cracks, we considered a problem of fibre-epoxy debonding (Chen and de Borst, 2022). The specimen geometry is shown in Fig. 7(a). Due to symmetry only one quarter of the specimen has been considered with symmetry-enforcing boundary conditions. Plane-strain conditions are assumed. The material properties are given as: for the fibre Young's modulus $E = 225$ GPa and Poisson's ratio $\nu = 0.2$, and for the epoxy Young's modulus $E = 4.3$ GPa and a Poisson's ratio $\nu = 0.34$. The Xu–Needleman cohesive zone law is used to describe the tractions at the fibre-epoxy interface, with $t_u = 50$ MPa and $\mathcal{G}_c = 4 \times 10^{-3}$ N/mm. The cohesive phase field method of Verhoosel and de Borst (2013) is employed to solve the displacement $\mathbf{u}$. In Fig. 7(a), the discrete interface Γ_c is regularised as a smeared interface Γ_ξ (blue area) by the phase field model in Section 3.1. The regularisation length is set as $\ell = 0.5$ μm. To demonstrate the capability of the proposed method two different triangular meshes are employed to triangulate the domain, see Fig. 7(b) and (c). To well describe Γ_ξ, the mesh around the interface Γ_c is refined with the smallest element size e.

The response curve, in terms of the horizontal stress σ_1 at point A as a function of the prescribed displacement $\bar{u}$, has been presented and validated in Chen and de Borst (2022), not shown here for brevity. The profile of the phase field and computed $\mathbf{u}\cdot\nabla d$ along the interface Γ_c are shown in Fig. 8(a) and (b). The phase-field variable is prescribed analytically by Eq. (14) (Chen and de Borst, 2022). $\mathbf{u}\cdot\nabla d$ is obtained from the solution of cohesive phase-field model. As expected, due to the narrow distribution of the phase field d, $\mathbf{u}\cdot\nabla d$ is confined to a local area around the crack. To obtain the crack opening displacement (COD), a line integral of $-2\mathbf{u}\cdot\nabla d$ is taken in the direction normal to the interface Γ_c, evaluated numerically by Gaussian quadrature. Fig. 9 compares the solutions of the proposed method against those of discrete interface model (Chen et al., 2017). It shows the results of two different triangular meshes. Clearly, the results agree well with the discrete interface solution. The smallest element size e shows only a slight deviation, due to the integral form of the proposed method. The integration Eq. (30) takes the information not only along the interface Γ_c, but also around the smeared area Γ_ξ.

6. Concluding remarks

The phase-field model is widely employed in the analysis of fracture due to its easy description of the crack and straightforward implementation. In the model, the crack is regularised and it has been applied to the analysis of brittle and cohesive fracture. In the brittle fracture model crack initiation and evolution are governed by a minimisation of a Griffith-like energy functional, while in the cohesive fracture model, the fracturing problem is ruled by minimising a crack displacement jump dependent energy functional. Obviously, the displacement jump, including the crack opening displacement $[\![\mathbf{u}\cdot\boldsymbol{n}]\!]$ and the displacement jump in the crack shear direction $[\![\mathbf{u}\cdot\boldsymbol{s}]\!]$, is essential in the cohesive fracture model and is also crucial in certain other applications, e.g. hydraulic fracturing. This study has focused on the derivation and verification of the computation of the crack opening displacement both for brittle and cohesive fracture models.

For the brittle fracture model the crack opening displacement $[\![\mathbf{u}\cdot\boldsymbol{n}]\!]$ can be approximated as a line integral of $\mathbf{u}\cdot\nabla d$ in the direction normal to the crack. Chukwudozie et al. (2019) have derived an identical form of $[\![\mathbf{u}\cdot\boldsymbol{n}]\!]$ and have verified its robustness by some benchmark cases. For the cohesive fracture model, the crack is regularised by using an approximated form of Dirac-delta function (δ_c) from the phase-field

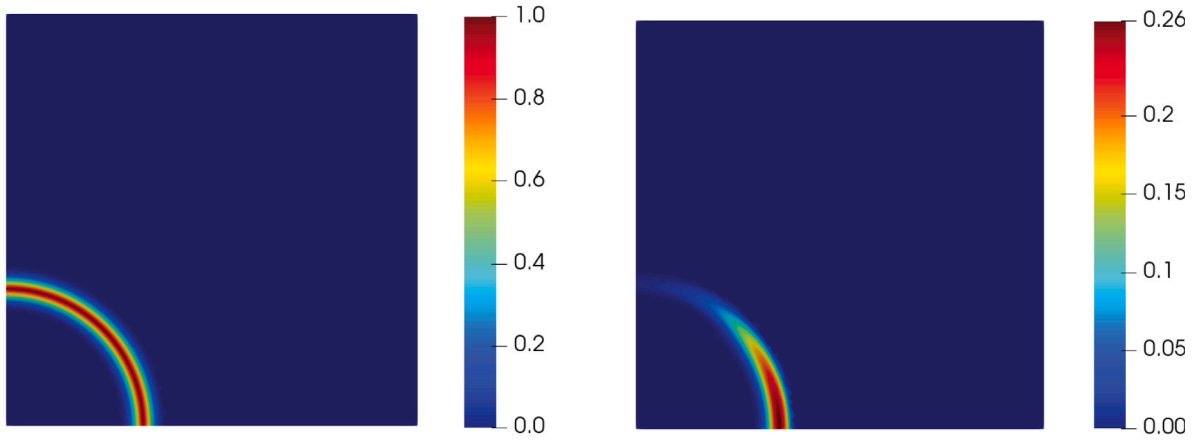

(a) contour plot of phase field d (b) contour plot of $\mathbf{u} \cdot \nabla d$ (μm)

Fig. 8. Plot of the phase field d and $\mathbf{u} \cdot \nabla d$ (μm) along the interface Γ_c at the loading step $\bar{u} = 0.25$ μm.

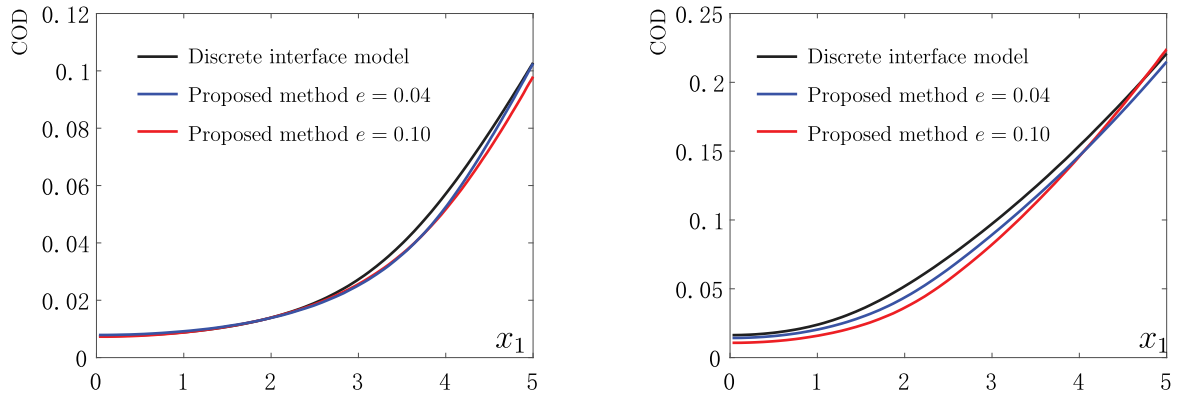

(a) at the loading step $\bar{u} = 0.15\mu$m. (b) at the loading step $\bar{u} = 0.25\mu$m

Fig. 9. Crack opening displacement (COD, μm) along the interface Γ_c at different loading steps. In the figure, the results of the domain triangulation in Fig. 7(b) and (c) are shown. The smallest element size e in Fig. 7(b) and (c) is $e = 0.10$ and $e = 0.04$ respectively. The discrete interface model is employed to provide the reference solution (Chen et al., 2017).

method. Herein, we have employed the gradient of the phase-field variable to define δ_c. A factor '2' is obtained in the form of δ_c, due to the identity constraint of the Dirac-delta function. This factor leads to a change in the form of the crack opening displacement $[\![\mathbf{u} \cdot \boldsymbol{n}]\!]$. It is given as a line integral of $2\mathbf{u} \cdot \nabla d$ in the direction normal to the crack. We have validated the proposed forms of the crack opening displacement analytically in a one-dimensional setting and numerically in two multi-dimensional problems, featuring straight crack and curved cracks.

Declaration of competing interest

The authors declare that they have no conflicts of interest regarding the manuscript.

Data availability

No data was used for the research described in the article

References

Alessi, R., Vidoli, S., De Lorenzis, L., 2018. A phenomenological approach to fatigue with a variational phase-field model: The one-dimensional case. Eng. Fract. Mech. 190, 53–73.

Barenblatt, G.I., 1962. The mathematical theory of equilibrium cracks in brittle fracture. Adv. Appl. Mech. 7, 55–129.

Bourdin, B., Chukwudozie, C., Yoshioka, K., 2012. A variational approach to the numerical simulation of hydraulic fracturing. In: SPE Annual Technical Conference and Exhibition. OnePetro, Richardson, TX.

Bourdin, B., Francfort, G.A., Marigo, J.-J., 2000. Numerical experiments in revisited brittle fracture. J. Mech. Phys. Solids 48, 797–826.

Bourdin, B., Francfort, G.A., Marigo, J.J., 2008. The variational approach to fracture. J. Elasticity 91, 5–148.

Chen, L., Bahai, H., Alfano, G., 2022. Extended Powell–Sabin finite element scheme for linear elastic fracture mechanics. Eng. Fract. Mech. 274, 108719.

Chen, L., de Borst, R., 2019. Cohesive fracture analysis using Powell–Sabin B-splines. Int. J. Numer. Anal. Methods Geomech. 43, 625–640.

Chen, L., de Borst, R., 2021. Phase-field modelling of cohesive fracture. Eur. J. Mech. A Solids 90, 104343.

Chen, L., de Borst, R., 2022. Phase-field regularised cohesive zone model for interface modelling. Theor. Appl. Fract. Mech. 103630.

Chen, L., Fathi, F., de Borst, R., 2022b. Hydraulic fracturing analysis in fluid-saturated porous medium. Int. J. Numer. Anal. Methods Geomech. 46, 3200–3216.

Chen, L., Li, B., de Borst, R., 2019. Energy conservation during remeshing in the analysis of dynamic fracture. Internat. J. Numer. Methods Engrg. 120, 433–446.

Chen, L., Li, B., de Borst, R., 2020. The use of Powell–Sabin B-splines in a higher-order phase-field model for crack kinking. Comput. Mech..

Chen, L., Lingen, E.J., de Borst, R., 2017. Adaptive hierarchical refinement of NURBS in cohesive fracture analysis. Internat. J. Numer. Methods Engrg. 112 (13), 2151–2173.

Chukwudozie, C., Bourdin, B., Yoshioka, K., 2019. A variational phase-field model for hydraulic fracturing in porous media. Comput. Methods Appl. Mech. Engrg. 347, 957–982.

Dugdale, D.S., 1960. Yielding of steel sheets containing slits. J. Mech. Phys. Solids 8, 100–104.

Fathi, F., Chen, L., de Borst, R., 2021. X-IGALME: Isogeometric analysis extended with local maximum entropy for fracture analysis. Internat. J. Numer. Methods Engrg. 122, 6103–6125.

Francfort, G.A., Marigo, J.-J., 1998. Revisiting brittle fracture as an energy minimization problem. J. Mech. Phys. Solids 46, 1319–1342.
Geuzaine, C., Remacle, J.-F., 2009. Gmsh: A 3-D finite element mesh generator with built-in pre-and post-processing facilities. Internat. J. Numer. Methods Engrg. 79, 1309–1331.
Ghaffari Motlagh, Y., de Borst, R., 2020. Considerations on a phase-field model for adhesive fracture. Internat. J. Numer. Methods Engrg. 121 (13), 2946–2963.
Heider, Y., 2021. A review on phase-field modeling of hydraulic fracturing. Eng. Fract. Mech. 253, 107881.
Khoei, A.R., 2014. Extended Finite Element Method: Theory and Applications. John Wiley & Sons.
Lee, S., Wheeler, M.F., Wick, T., 2017. Iterative coupling of flow, geomechanics and adaptive phase-field fracture including level-set crack width approaches. J. Comput. Appl. Math. 314, 40–60.
Li, T., Marigo, J.-J., Guilbaud, D., Potapov, S., 2016. Gradient damage modeling of brittle fracture in an explicit dynamics context. Internat. J. Numer. Methods Engrg. 108 (11), 1381–1405.
May, S., Vignollet, J., de Borst, R., 2015. A numerical assessment of phase-field models for brittle and cohesive fracture: Γ-convergence and stress oscillations. Eur. J. Mech. A Solids 52, 72–84.
Miehe, C., Hofacker, M., Schänzel, L.-M., Aldakheel, F., 2015. Phase field modeling of fracture in multi-physics problems. Part II. Coupled brittle-to-ductile failure criteria and crack propagation in thermo-elastic–plastic solids. Comput. Methods Appl. Mech. Engrg. 294, 486–522.
Miehe, C., Mauthe, S., 2016. Phase field modeling of fracture in multi-physics problems. Part III. Crack driving forces in hydro-poro-elasticity and hydraulic fracturing of fluid-saturated porous media. Comput. Methods Appl. Mech. Engrg. 304, 619–655.
Nguyen, T.T., Yvonnet, J., Zhu, Q.-Z., Bornert, M., Chateau, C., 2016. A phase-field method for computational modeling of interfacial damage interacting with crack propagation in realistic microstructures obtained by microtomography. Comput. Methods Appl. Mech. Engrg. 312, 567–595.
Sneddon, I., Lowengrub, M., 1969. Crack Problems in the Classical Theory of Elasticity. John Wiley & Sons, Chichester.
Verhoosel, C.V., de Borst, R., 2013. A phase-field model for cohesive fracture. Internat. J. Numer. Methods Engrg. 96, 43–62.
Vignollet, J., May, S., de Borst, R., Verhoosel, C.V., 2014. Phase-field models for brittle and cohesive fracture. Meccanica 49, 2587–2601.
Wheeler, M.F., Wick, T., Wollner, W., 2014. An augmented-Lagrangian method for the phase-field approach for pressurized fractures. Comput. Methods Appl. Mech. Engrg. 271, 69–85.
Xu, X.P., Needleman, A., 1993. Void nucleation by inclusion debonding in a crystal matrix. Modelling Simul. Mater. Sci. Eng. 1, 111–132.
Yoshioka, K., Naumov, D., Kolditz, O., 2020. On crack opening computation in variational phase-field models for fracture. Comput. Methods Appl. Mech. Engrg. 369, 113210.